Available online at www.sciencedirect.com

SciVerse ScienceDirect

Ceramics International 38 (2012) 1391–1398

CERAMICS INTERNATIONAL

www.elsevier.com/locate/ceramint

Raman scattering, electronic structure and microwave dielectric properties of $Ba([Mg_{1-x}Zn_x]_{1/3}Ta_{2/3})O_3$ ceramics

Ping-Fan Ning, Ling-Xia Li *, Ping Zhang, Wang-Suo Xia

School of Electronic and Information Engineering, Tianjin University, Tianjin 300072, China

Received 7 August 2011; received in revised form 6 September 2011; accepted 6 September 2011
Available online 14 September 2011

Abstract

Effects of Zn substitution for Mg on the crystal structure, lattice vibrations and microwave dielectric properties of $Ba(Mg_{1/3},Ta_{2/3})O_3$ (BMT) ceramics were investigated. Raman scattering spectra for $Ba([Mg_{1-x}Zn_x]_{1/3}Ta_{2/3})O_3$ (BMZT) ceramics, with $x = 0$, 0.2, 0.4, 0.6, 0.8 and 1.0, were measured at room temperature. The Raman result shows a dominance of 1:2 ordered structure at all Zn substitution contents. All Raman modes shift to lower frequencies with increasing Zn substitution. Higher *Qf* value correlates well with narrower width of the breathing Raman mode $A_{1g}(4)$ and larger relative intensity of 1:2 long-range-ordered mode $E_g(2)$ in BMZT solid solution. First-principle calculation was performed to investigate the electronic structure of 1:2 ordered BMT and $Ba(Zn_{1/3},Ta_{2/3})O_3$ (BZT). Covalent bond between Zn and O in BZT is much stronger than that between Mg and O in BMT due to the Zn 3*d* orbital. Zn substitution for Mg leads to longer and weaker Ta–O bonds, which may be one reason for the variation of Raman spectroscopy and microwave dielectric properties of BMZT system.

Keywords: B. Spectroscopy; C. Dielectric properties; D. Perovskites; D. Tantalates

1. Introduction

Complex perovskite ceramics with general formula $Ba(B'_{1/3}B''_{2/3})O_3$ (B' = Mg, Ni, and Zn and B'' = Nb and Ta), which exhibit excellent microwave dielectric properties: high permittivity, low loss tangent and near zero temperature coefficient of resonant frequency, are currently being used as dielectric resonators for microwave and millimeter wave technologies [1–5]. Experimental and theoretical studies about these materials have been extensively conducted over the past several decades [4–8]. Recently, the study of phonon vibration spectra of $Ba(B'_{1/3}B''_{2/3})O_3$ has been of particular interest for the dielectric properties at microwave frequencies are mainly contributed from the ionic polarization. Far-IR and Raman spectra are useful and complementary to analyze lattice vibrations. Tamura et al. first analyzed the vibration of 1:2 ordered $Ba(Zn_{1/3},Ta_{2/3})O_3$ (BZT) normal modes [9]. Siny et al. investigated the Raman spectra of $Ba(Mg_{1/3},Ta_{2/3})O_3$ (BMT) measured at different temperatures, proposing the existence of 1:1 ordered structure of the Mg^{2+} and Ta^{5+} cations in some nanoscale regions [10]. Moreira et al. discussed the 1:2 ordering degree of BMT based on the Raman and X-ray techniques [11]. Very recently, Wang et al. systematically studied Raman spectra of ordered BMT and assigned the peaks based on the result of first principle calculation [12]. Besides, Dai et al. studied electronic structure, phonon structure and dielectric properties of $Ba(Zn_{1/3}Nb_{2/3})O_3$, $Ba(Mg_{1/3}Nb_{2/3})O_3$ and BMT [13,14].

It is well known that lattice vibrations and microwave dielectric properties are significantly affected by ionic substitutions. Chia et al. studied the normal modes of $xBa(Mg_{1/3}Ta_{2/3})O_3$–$(1-x)Ba(Mg_{1/3}Nb_{2/3})O_3$ ceramics and correlated the lattice vibration characteristics with the dielectric properties of the materials [15]. Surendran and Sebastian investigated the crystal structure and microwave dielectric properties of $Ba([Mg_{1-x}Zn_x]_{1/3}Ta_{2/3})O_3$ (BMZT) solid solution without mentioning lattice vibration [16]. Shimada studied the effects of Zn and Ni substitution for Mg in BMT on the microwave dielectric properties and lattice vibrations using Far-IR spectra [17,18]. Chen and Chia et al. investigated the effect of small amount of nickel doping on the structural and microwave properties of $Ba(Mg_{1/3}Ta_{2/3})O_3$ by the Raman scattering, EXAFS and X-ray diffraction methods [19].

* Corresponding author. Tel.: +86 22 2740 2838; fax: +86 22 2740 1233.
E-mail address: llxtju@126.com (L.-X. Li).

0272-8842/$36.00
doi:10.1016/j.ceramint.2011.09.018

However, there is little systematical investigation about the effects of Mg site substitution on Raman modes for 1:2 ordered BMT. And the origin of the variation of the dielectric properties with increase of Zn substitution to Mg site in BMZT solid solution is not clear.

In the present study, BMZT samples with different contents of Zn substitution were synthesized. And the variation of Raman mode and microwave dielectric properties caused by Zn substitution for Mg was investigated. We attempted to find the origin of the change in the Raman modes for BMZT by calculating the electronic structure of BMT and BZT using first-principle approach.

2. Experimental procedure and calculation

The $Ba([Mg_{1-x}Zn_x]_{1/3}Ta_{2/3})O_3$ ($x = 0$, 0.2, 0.4,0.6, 0.8, 1) ceramics were prepared by the conventional solid-state reaction method. High purity $BaCO_3$, MgO, ZnO and Ta_2O_5 were used as the starting materials. Because MgO is hygroscopic, it was first fired at 600 °C to avoid moisture retention. Stoichiometric raw materials were mixed by ball milling in deionized water with agate balls for 24 h. The resulted slurry was then dried at 100 °C and calcined for 4 h at 1300 °C in air. Again, the calcined powders were ball milled in deionized water for 12 h. The ground powders were granulated with PVA and pressed into pellets of about 10 mm diameter and 5 mm thickness under a pressure of 100 MPa using uniaxial pressing. The samples were sintered at 1500–1600 °C for 6 h in air.

XRD patterns were collected on a Rigaku X-ray diffractometer (Model D/MAX-B, Rigaku Co., Japan) using Ni filtered CuKα radiation (λ = 0.1542 nm) at 40 kV and 40 mA settings. Morphology of samples was observed by a field emission scanning electron microscopy (Model JSM-7600F, JEOL Ltd., Japan). Raman measurements were carried out at room temperature, and the signals were recorded by a DXR Raman Microscope (DXR Microscope, ThermoFisher, USA). The 100-mW output of the 532-nm line of an Nd YAG laser was used as the excitation source. The obtained Raman spectra were recorded with a resolution approximately 1 cm^{-1}.

An HP8720ES vector network analyzer (Hewlett-Packard, Santa Rosa, CA) was used for the measurement of microwave dielectric properties. The dielectric constants were measured using the Hakki and Coleman's open resonator method. The unloaded quality factors were evaluated using the cavity method. The temperature coefficients of the resonant frequency τ_f were calculated from the data collected at the temperature range of 25–85 °C according to $\tau_f = (f_{85} - f_{25})/(f_{25} \times 60)$, where f_{25} and f_{85} are the resonant frequencies at 25 °C and 85 °C, respectively. All the measurements were made in the frequency range of 7–9 GHz.

We performed first-principle calculations to investigate electronic structure of BMT and BZT using CASTEP (Cambridge Serial Total Energy Package) software package, which is a plane wave pseudo-potential method. A 15-atom unit cell was used for both BMT and BZT in calculation. For the calculations, the density functional theory (DFT) was used, in which plane wave basis set was chosen for the expansion of valance-electron wave functions at the local density approximation (LDA) level. The initial structures of 1:2 ordered BMT and BZT were obtained from Lufaso's work [20] and Bieringer's work [21] respectively and then relaxed by the Broyden–Fletcher–Goldfarb–Shanno quasi-Newton scheme (BFGS) method. Energy cut off value of plane wave basis set was selected as 650 eV and the criterion for self-consistency was eigenenergy convergence within 10^{-8} eV/atom. The k-point set was chosen as $5 \times 5 \times 4$ Monkhorst–Pack grid and the pseudopotential was constructed from the CASTEP database.

3. Results and discussion

XRD patterns for BMZT are presented in Fig. 1. For this ceramic system, solid solutions were formed in the full-range composition and no apparent secondary phase was produced. According to the theory of X-ray diffraction, the relation between the interplanar spacing ($d_{h\,k\,l}$) and the diffraction angle (θ) can be expressed as follows:

$$\lambda = 2d_{h\ k\ l} \sin\ \theta \tag{1}$$

For hexagonal structure, the lattice parameter of a given plane with Miller indices ($h\,k\,l$) can be derived using the equation:

$$\frac{1}{d^2_{h\ k\ l}} = \frac{4}{3}\left(\frac{h^2 + hk^2 + k^2}{a^2}\right) + \frac{l^2}{c^2} \tag{2}$$

where a and c are lattice parameters. The results of the calculations for the various samples are presented in Table 1. The observed trend in the increase in cell volume with increasing Zn content, depicted in Fig. 2, is expected since the ionic radius of Zn^{2+} is larger than that of Mg^{2+} [22]. The 1:2 long-range ordered arrangements of the cations along the ⟨1 1 1⟩ direction in BMT might be affected by Zn doping due to the electrostatic interactions between Mg/Zn and Ta. The ordering parameters of BMT and BZT can be calculated using the following two expressions respectively [16,19,23]:

$$S_{BMT} = \sqrt{\frac{(I_{1\ 0\ 0}/I_{1\ 1\ 0,1\ 0\ 2})_{observed}}{(8.7/100)}} \tag{3}$$

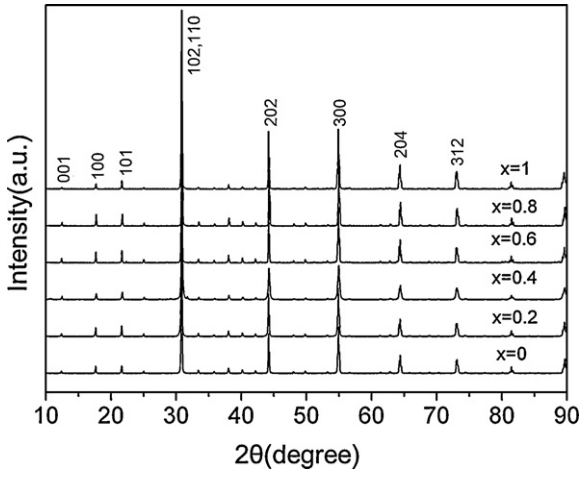

Fig. 1. X-ray diffraction patterns of $Ba([Mg_{1-x}Zn_x]_{1/3}Ta_{2/3})O_3$ ceramics.

Table 1
Unit cell properties of $Ba([Mg_{1-x}Zn_x]_{1/3}Ta_{2/3})O_3$ solid solution phases.

x	a (Å)	c (Å)	Cell volume (Å^3)
0	5.7824	7.0877	205.2354
0.2	5.7875	7.0834	205.4728
0.4	5.7851	7.0922	205.5575
0.6	5.7835	7.1010	205.6987
0.8	5.7882	7.1022	206.0680
1	5.7917	7.1039	206.3667

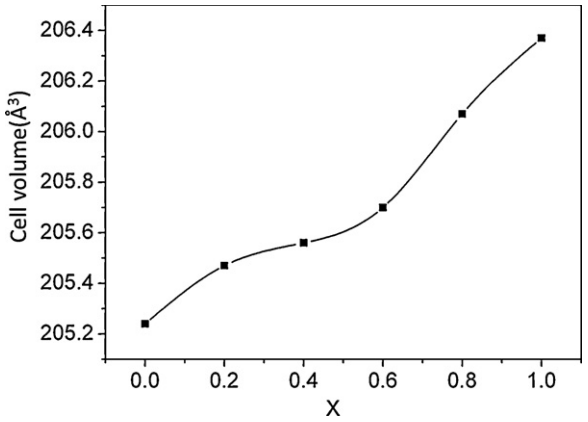

Fig. 2. Variation of cell volume with composition for $Ba([Mg_{1-x}Zn_x]_{1/3}Ta_{2/3})O_3$ ceramics.

$$S_{BZT} = \sqrt{\frac{(I_{1\ 0\ 0}/I_{1\ 1\ 0,1\ 0\ 2})_{observed}}{(3.7/100)}} \quad (4)$$

In which $(I_{1\ 0\ 0}/I_{1\ 1\ 0,\ 1\ 0\ 2})_{observed}$ represents the ratio of the integral intensity of super structural reflection line 1 0 0 to that of 1 1 0 and 1 0 2 line calculated from XRD patterns. Thus the cation ordering degrees of solid solution phase between BMT and BZT are calculated using the empirical relation [16]:

$$S = (1 - x)S_{BMT} + xS_{BZT} \quad (5)$$

The calculated ordering degree (S) for the BMZT ceramics are shown in Fig. 3, from which it is clear that the solid solution phase is of high cation ordering degree.

Figs. 3 and 4 show the microwave dielectric properties of BMZT ceramics. The Qf value of BMZT with various Zn substitution content are plotted in Fig. 3. The Qf value of pure

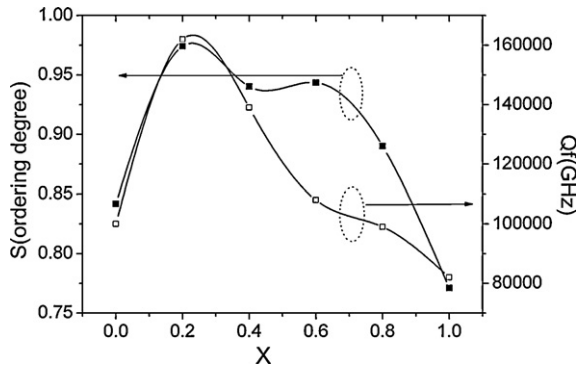

Fig. 3. Variation of ordering degree S and Qf values with composition for $Ba([Mg_{1-x}Zn_x]_{1/3}Ta_{2/3})O_3$ ceramics.

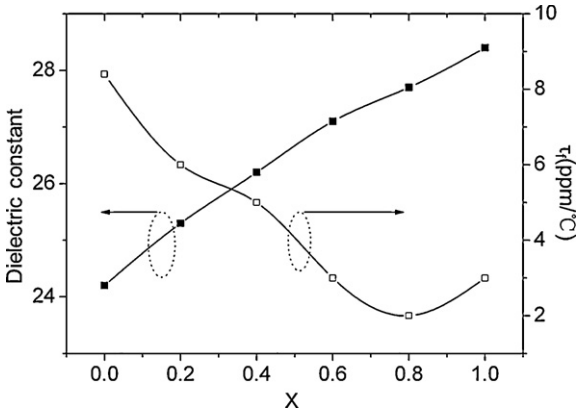

Fig. 4. Variation of τ_f and dielectric constant with composition for $Ba([Mg_{1-x}Zn_x]_{1/3}Ta_{2/3})O_3$ ceramics.

BMT and BZT are 100,200 GHz and 80,500 GHz respectively. The quality factor reaches a maximum (Qf = 160, 500 GHz) for $Ba(Mg_{0.8}Zn_{0.2})_{1/3}Ta_{2/3}O_3$. When the substitution level of Zn at Mg site is greater than x = 0.2, the dielectric loss increases. In a previous study, Shimada reported that the dielectric loss monotonically increases with Zn substitution content, which was different from our result [17]. Generally, ordering degree of B site ions in BMT was correlated with sintering time. The sintering time in Shimada's report was 50 h which was much longer than that in this work (6 h). This significant difference of

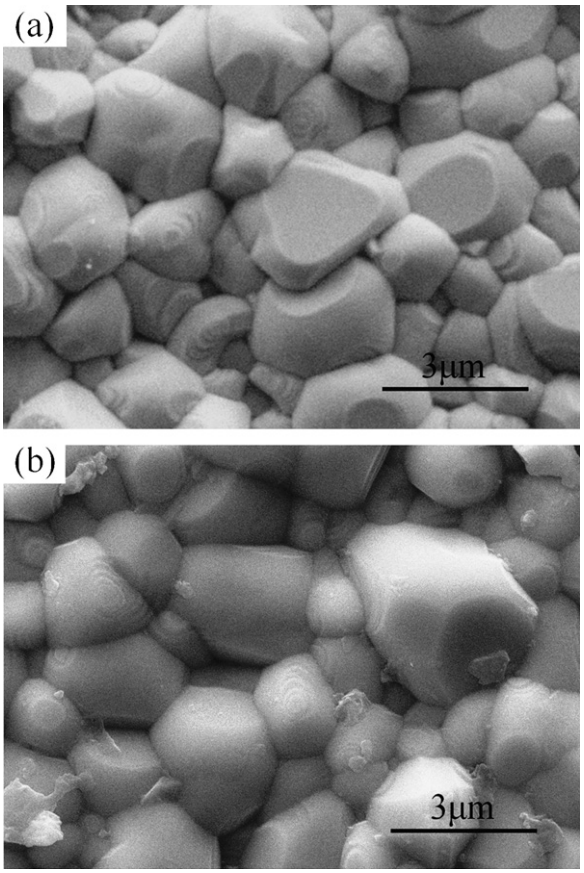

Fig. 5. Scanning electron microscopy photographs of as-sintered $Ba([Mg_{1-x}Zn_x]_{1/3}Ta_{2/3})O_3$ ceramics: (a) x = 0, and (b) x = 0.2.

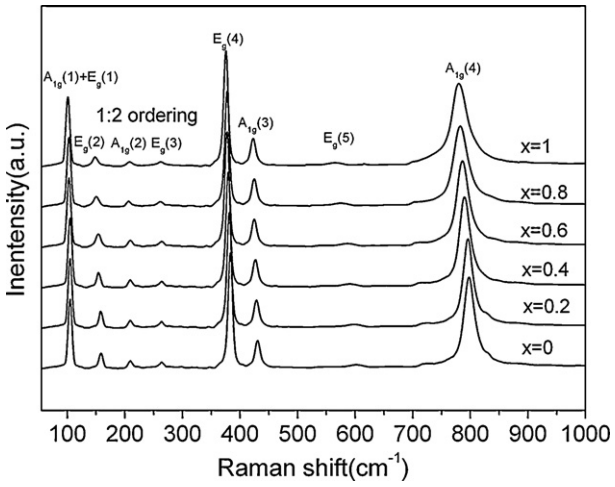

Fig. 6. Raman spectra of $Ba([Mg_{1-x}Zn_x]_{1/3}Ta_{2/3})O_3$ ceramics.

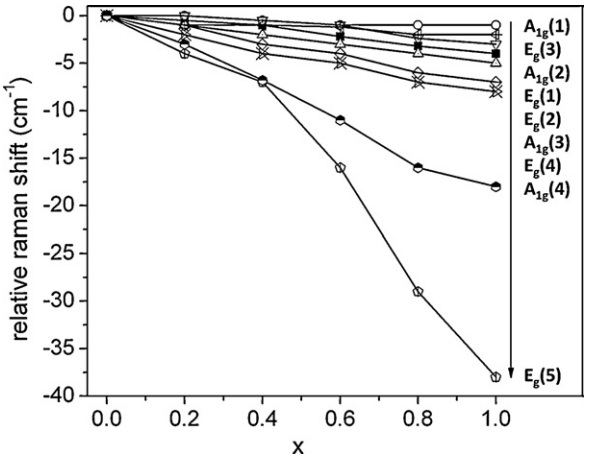

Fig. 7. Variation of relative Raman shift with composition for $Ba([Mg_{1-x}Zn_x]_{1/3}Ta_{2/3})O_3$ ceramics.

sintering process might be the reason for the difference in dielectric properties. It should be noted that the variation of *Qf* with Zn content consists well with that of ordering degree *S* in BMZT solid solution (Fig. 3). As depicted in Fig. 4, the dielectric constant of BMZT increased from 24.8 ($x = 0$) to 29.7 ($x = 1$). The elevation of the permittivity of BMZT with increasing Zn substitution can be ascribed to the formation of the solid solution phase and the greater ionic polarizability of Zn than Mg. The temperature coefficient of resonant frequency decreased with increasing Zn content (Fig. 4). The variation of the temperature coefficient of resonant frequency of the solid solution is between 9 ppm/°C and 2 ppm/°C.

The microwave dielectric loss can be affected by the intrinsic factors such as lattice vibration and the extrinsic

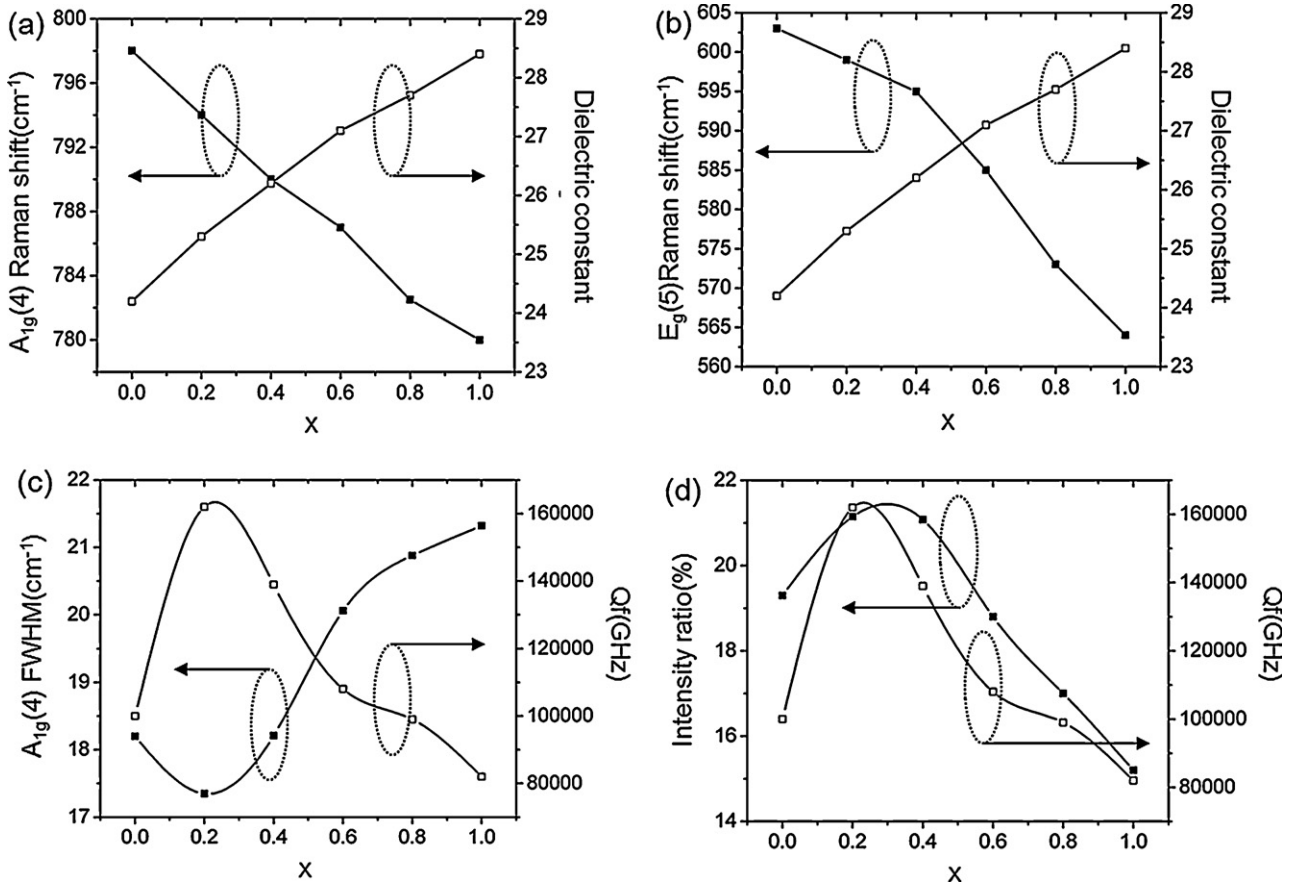

Fig. 8. Zn-concentration dependence of the characteristics of phonons and the microwave properties of the $Ba([Mg_{1-x}Zn_x]_{1/3}Ta_{2/3})O_3$ ceramics. (a) The Raman shift of $A_{1g}(4)$ mode and the dielectric constant, (b) the Raman shift of $E_g(4)$ mode and the dielectric constant, (c) FWHM of $A_{1g}(4)$ mode and the *Qf* value, and (d) normalized intensity of 1:2 ordered phonon, $E_g(2)$, and the *Qf* value are plotted with *x*.

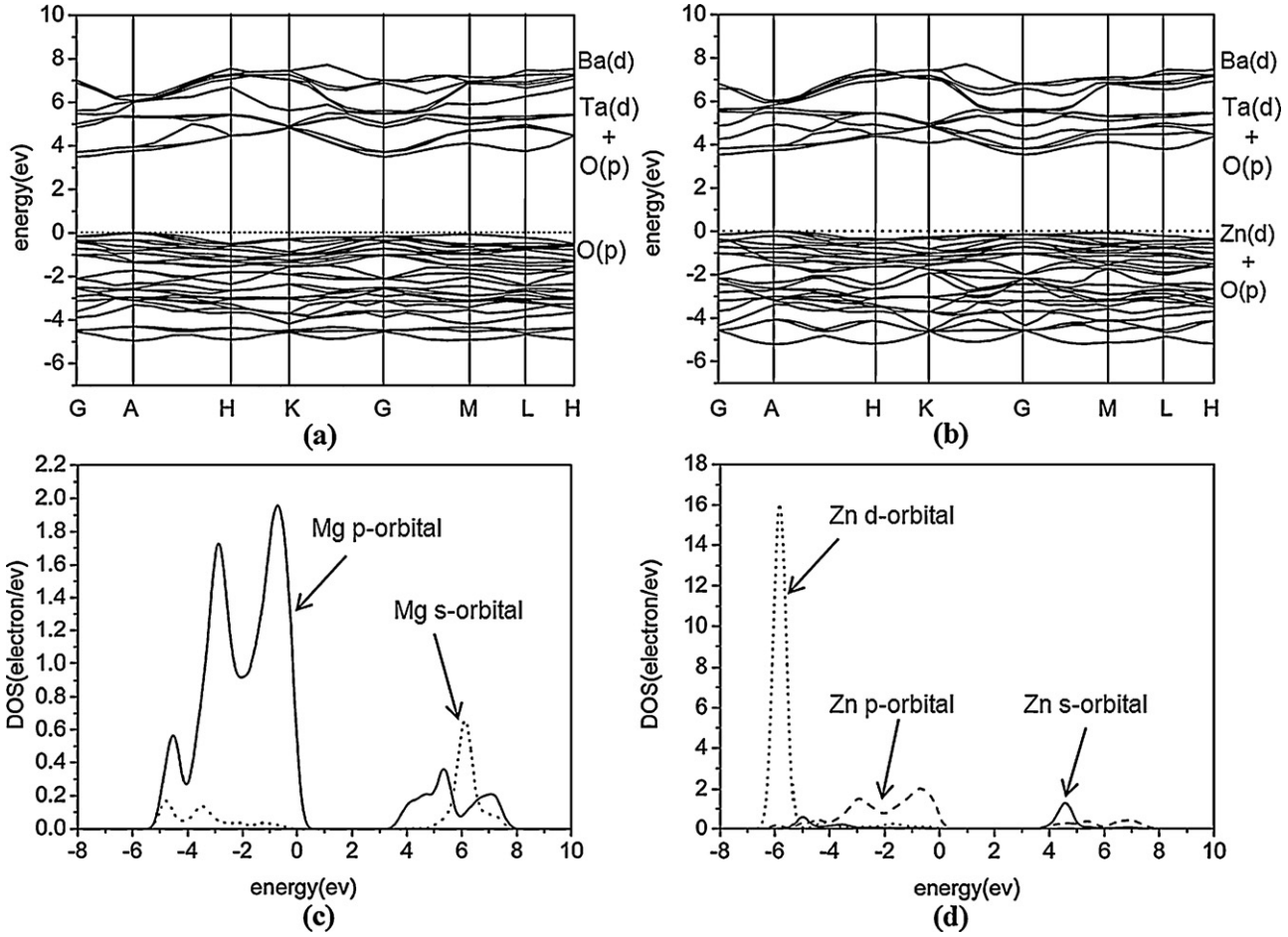

Fig. 9. (a) Band structures of BMT, (b) band structures of BZT, (c) partial DOS of BMT for Mg, and (d) partial DOS of BZT for Zn.

factors such as bulk density, secondary phase, grain size, and so on. Relative density of all samples in this paper was higher than 95% and no apparent secondary phase was detected in all samples by XRD. Fig. 5 shows the SEM micrographs of the BMT and $Ba(Mg_{0.8}Zn_{0.2})_{1/3}Ta_{2/3}O_3$ samples sintered for 6 h at 1600 °C. There is no significant difference in grain size between two samples, while the *Qf* values of the BMT and $Ba(Mg_{0.8}Zn_{0.2})_{1/3}Ta_{2/3}O_3$ are 100,000 GHz and 160,000 GHz respectively. Obviously, the extrinsic factors such as bulk density, secondary phase, grain size, and so on are not the dominant factors affecting the microwave dielectric loss in this system. For further understanding the effects of Zn substitution, Raman scattering spectroscopy of BMZT were measured and analyzed.

The 1:2 ordered structure of BMT belongs to $P\bar{3}m1(D_{3d}^3)$ space group, and its unit cell has 15 atoms. With the consultation of the Bilbao Crystallographic Center website (www.cryst.ehu.es), total optical modes are $4A_{1g} + A_{2g} + 5E_g + 2A_{1u} + 7A_{2u} + 9E_u$, in which $4A_{1g} + 5E_g$ are Raman active, and $7A_{2u} + 9E_u$ are IR active [24]. Based on the notation of Wychkoff site and factor group analysis, nine Raman active modes, $4A_{1g} + 5E_g$, are related only to the motion of Ba and Ta atoms at the 2*d* site and the motion of O atoms at the 6*i* site. Although Mg atoms at 1*b* site do not contribute to Raman active modes directly according to group theory analysis, Zn substitution for Mg changes the electronic structure and bonding status in BMT. Thus, it is inferred that the variation in lattice vibration brought by Zn substitution can be manifested by Raman scattering spectroscopy.

Fig. 6 depicts the Raman spectra of BMZT ceramics at room temperature. Raman peaks are of narrow line width, which is intimately correlated with highly ordered structure and high Q characteristics of the materials [25]. Most of the peaks can be assigned to the nine Raman active modes, $4A_{1g} + 5E_g$, and separated into three groups: [10,12,15] (i) modes $A_{1g}(1)$ and $E_g(1)$ correlated with the vibrations of Ba atoms near 105 cm^{-1}, (ii) 1:2 ordered phonon modes $E_g(2)$, $A_{1g}(2)$ and $E_g(3)$ dominated by the vibrations of Ta atoms in the range of 150–300 cm^{-1}, and (iii) modes $E_g(4)$, $A_{1g}(3)$, $E_g(5)$ and $A_{1g}(4)$ contributed by the vibrations of the oxygen octahedral in the range of 350–800 cm^{-1}. Besides, three weak peaks, M_1 near $E_g(4)$, M_2 and M_3 around $A_{1g}(4)$ were identified. These extra modes might be caused by distortion of TaO_6 octahedron or defects in samples [11,26,27].

As is shown in Fig. 7, all phonon modes shift to lower frequencies with increasing Zn substitution. The frequencies of five phonons $A_{1g}(1)$, $E_g(1)$, $E_g(2)$, $A_{1g}(2)$ and $E_g(3)$ are slightly impacted by the amount of Zn substitutions. The Ba and Ta vibrations are relatively insensitive to the Zn concentration. Phonon modes $E_g(4)$, $A_{1g}(3)$, $E_g(5)$ and $A_{1g}(4)$ are significantly

red-shifted as the amount of Zn increases. The modes $A_{1g}(3)$ and $A_{1g}(4)$ are dominated by breath-vibrations of oxygen octahedron. And the modes $E_g(4)$ and $E_g(5)$ are dominated by the twisting breath-vibrations of oxygen octahedron with different relative vibration directions [12]. The vibrations of oxygen at 6*i* site are significantly influenced by Zn contents due to the different bond energy between Zn–O bond and Mg–O bond.

Fig. 8a and b shows the compositional dependence of the dielectric constant and Raman shift of $A_{1g}(4)$ mode and $E_g(5)$mode. The $E_g(5)$ mode around 603 cm^{-1} and $A_{1g}(4)$ mode around 798 cm^{-1} shift downward and the dielectric constant increases with increasing Zn content. The lower normal mode frequency of TaO_6 octahedral cages caused by Zn substitution indicates that the Ta–O bonds became weaker with Zn increasing. Higher dielectric constant is due to the expanded TaO_6 octahedral cages and larger polarizability of Zn^{2+} than Mg^{2+}. In Fig. 8c, the full width at half maximum (FWHM) of the $A_{1g}(4)$ mode and the *Qf* value are plotted as a function of Zn substitution and the correlation between the FWHM and *Qf* value is clearly identified. Large phonon width indicates a poor crystalline structure and a short phonon lifetime [26]. Similarly, the low value of *Qf* implies a short distance of microwave propagation. Therefore, the width of $A_{1g}(4)$ mode reflects the propagation property of the phonon in three-dimensional oxygen octahedral network, while the propagation of microwave strongly depends on the properties of the oxygen octahedron, as indicated in Fig. 8c. In Fig. 8d, the *Qf* value and the Raman intensity of the 1:2 ordered $E_g(2)$ mode normalized to $E_g(4)$ mode as a function of x are plotted. The intensity of the 1:2 ordered phonons correlate well with the *Qf* values. The

Table 2
Relaxed structure parameters and bond lengths of BMT and BZT.

Properties	BMT	BZT
a (Å)	5.7739	5.7830
c (Å)	7.0938	7.1076
v ($Å^3$)	204.804	205.854
Mg/Zn–O^1 (Å)	2.1175	2.2195
Ta–O^1 (Å)	1.8678	1.8706
Ta–O^2 (Å)	2.0167	2.0523

Mg/Zn, Ta, O^1 and O^2 are in sites 1*b*, 2*d*, 6*i* and 3*f* respectively.

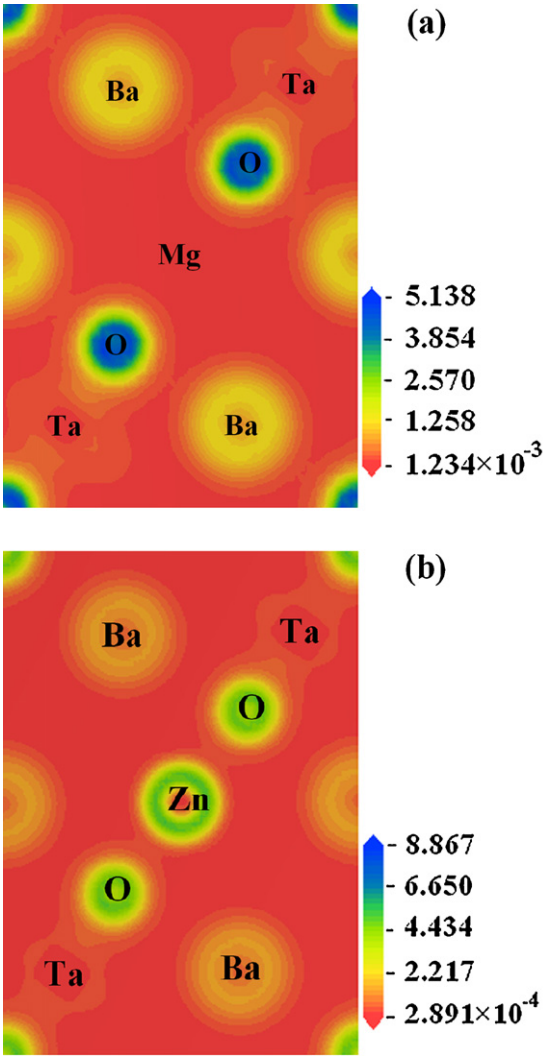

Fig. 10. The total electron density patterns of BMT (a) and BZT (b).

decrease in the intensity of 1:2 ordered phonons implies the degradation of the 1:2 ordered structure, in turn, lowers the microwave *Qf* value. This result obtained by Raman scattering is consistent with that given by XRD as shown in Fig. 3.

The electronic structures of 1:2 ordered (164) BMT and BZT were calculated using DFT method. Although lattice parameters and cell volume of BMZT can be obtained from XRD data, as illustrated in Table 1, the accurate position of O atoms at 6*i* site is difficult to determine using XRD [20]. So, the neutron powder diffraction data from Lufaso's work [20] and Bieringer's work [21] were used for computer simulation. Table 2 shows the relaxed structure parameters and bond lengths of BMT and BZT. The volume of unit cell of BZT is slightly larger than that of BMT, which is consistent with XRD result (Fig. 2). Bond lengths of Zn–O^1, Ta–O^1 and Ta–O^2 in BZT are longer than that of Mg–O^1, Ta–O^1 and Ta–O^2 in BMT. Typically, phonon energies change inversely with the bond distance. Therefore, the Raman phonon modes shift to lower frequencies with increasing Zn content as shown in Fig. 7. Fig. 9 presents band structure of BMT and BZT as well as the partial density of states (PDOS) of Mg and Zn. The most conspicuous difference in electronic structure between BMT and BZT is Zn 3*d*-orbitals. It is predicted that the significant charge transfer between the cation *d*-orbitals will provide a degree of covalent directional bonding between atoms [28]. In BZT, our calculation indicates that charge is transferred from Ta 5*d* levels in the bottom of conduction band to Zn 3*d* levels near the valence band edge, see Fig. 9. There is no similar charge transfer in BMT due to the absence of *d*-orbital in Mg. The total electron density patterns of BMT and BZT are illustrated in Fig. 10. The covalent interaction among Zn, O, and Ta are distinctly shown in Fig. 10a, but no obvious covalent interaction between Mg and O is observed in Fig. 10b. Such covalent interaction is closely related with the Zn 3*d*-orbital. Covalent bonds between Zn and O originate from the hybridizations of Zn 3*d*-orbital and O 2*p*-orbital. It is notable in Fig. 10 that the covalent interaction between Ta and O in BZT is less intensive than that in BMT, which leads to weaker and longer Ta–O bond in BZT.

4. Conclusions

Highly ordered BMZT ceramics were prepared by conventional solid-state reaction method. Crystal structure, Raman spectra and microwave properties were discussed. Zn substitutions lead to increased cell volume of the BMT. Phonon modes $E_g(4)$, $A_{1g}(3)$, $E_g(5)$ and $A_{1g}(4)$ associated with the vibration of oxygen octahedron are significantly red-shifted as the amount of Zn increases. The permittivity increased with Zn substitution for Mg due to the larger polarizability of Zn and the decrease in the frequencies of the oxygen octahedron breathing vibrations ($E_g(5)$ and $A_{1g}(4)$ modes). The variation of *Qf* value with increasing Zn substitution correlates well with the variation of order parameter *S*, FWHM of $A_{1g}(4)$ mode and normalized intensity of 1:2 ordered mode $E_g(2)$. Electronic structure of BMT and BZT was calculated using DFT method. Covalent bond between Zn and O in BZT is much stronger than that between Mg and O in BMT. The origin of the covalent bond Zn–O is the hybridization of Zn 3d orbital and O 2p orbital. Zn substitution for Mg leads to longer and weaker Ta–O bonds, which may be one reason for variation of Raman spectroscopy and microwave dielectric properties in BMZT system.

Acknowledgments

This work was supported financially by Program for New Century Excellent Talents in University (NCET) and 863 program (2007AA03Z423) and China Postdoctoral Science Foundation. Gratitude is expressed to Advanced Instrumental Detecting & Analytical Center, School of Chemical Engineering and Technology, Tianjin University, for providing access to the Materials Studio molecular modeling software.

References

[1] R.J. Cava, Dielectric materials for applications in microwave communications, J. Mater. Chem. 11 (2001) 54–65.
[2] I.M. Reaney, D. Iddles, Microwave dielectric ceramics for resonators and filters in mobile phone networks, J. Am. Ceram. Soc. 89 (2006) 2063–2072.
[3] M.T. Sebastian, Dielectric Materials for Wireless Communication, Elsevier Science Technology Publications, Oxford, 2008.
[4] S. Nomura, K. Toyama, K. Kaneta, $Ba(Mg_{1/3}Ta_{2/3})O_3$ ceramics with temperature stable high dielectric constant and low microwave loss, Jpn. J. Appl. Phys. 21 (1982) L624–L626.
[5] S. Kawashima, M. Nishida, I. Ueda, H. Ouchi, $Ba(Zn_{1/3}Ta_{2/3})O_3$ ceramics with low dielectric loss at microwave frequencies, J. Am. Ceram. Soc. 66 (1983) 421–423.
[6] D.J. Barber, K.M. Moulding, J. Zhou, M. Li, Structural order in $Ba(Zn_{1/3}Ta_{2/3})O_3$, $Ba(Zn_{1/3}Nb_{2/3})O_3$ and $Ba(Mg_{1/3}Ta_{2/3})O_3$ microwave dielectric ceramics, J. Mater. Sci. 32 (1997) 1531–1544.
[7] N. Ichinose, T. Shimada, Effect of grain size and secondary phase on microwave dielectric properties of $Ba(Mg_{1/3}Ta_{2/3})O_3$ and $Ba([Mg,Zn]_{1/3}Ta_{2/3})O_3$ systems, J. Eur. Ceram. Soc. 26 (2006) 1755–1759.
[8] T. Shimada, K. Ichikawa, T. Minemura, T. Kolodiazhnyi, J. Breeze, N.M. Alford, G. Annino, Temperature and frequency dependence of dielectric loss of $Ba(Mg_{1/3}Ta_{2/3})O_3$ microwave ceramics, J. Eur. Ceram. Soc. 30 (2010) 331–334.
[9] H. Tamura, D.A. Sagala, K. Wakino, Lattice-vibrations of $Ba(Zn_{1/3}\ Ta_{2/3})O_3$ crystal with ordered perovskite structure, Jpn. J. Appl. Phys. 25 (1986) 787–791.
[10] I.G. Siny, R. Tao, R.S. Katiyar, R. Guo, A.S. Bhalla, Raman spectroscopy of Mg–Ta order–disorder in $BaMg_{1/3}Ta_{2/3}O_3$, J. Phys. Chem. Solids 59 (1998) 181–195.
[11] R.L. Moreira, F.M. Matinaga, A. Dias, Raman-spectroscopic evaluation of the long-range order in $Ba(B_{1/3}'B_{2/3}'')O_3$ ceramics, Appl. Phys. Lett. 78 (2001) 428–430.
[12] C.H. Wang, X.P. Jing, L. Wang, J. Lu, XRD and Raman studies on the ordering/disordering of $Ba(Mg_{1/3}Ta_{2/3})O_3$, J. Am. Ceram. Soc. 92 (2009) 1547–1551.
[13] Y. Dai, G. Zhao, H. Liu, First-principles study of the dielectric properties of $Ba(Zn_{1/3}Nb_{2/3})O_3$ and $Ba(Mg_{1/3}Nb_{2/3})O_3$, J. Appl. Phys. 105 (2009) 034111.
[14] Y. Dai, G. Zhao, L. Guo, H. Liu, First-principles study of the difference in permittivity between $Ba(Mg_{1/3}Ta_{2/3})O_3$ and $Ba(Mg_{1/3}Nb_{2/3})O_3$, Solid State Commun. 149 (2009) 791–794.
[15] C.T. Chia, Y.C. Chen, H.F. Cheng, Correlation of microwave dielectric properties and normal vibration modes of $xBa(Mg_{1/3}Ta_{2/3})O_3$–$(1-x)Ba(Mg_{1/3}Nb_{2/3})O_3$ ceramics: I Raman spectroscopy, J. Appl. Phys. 94 (2003) 3360–3364.
[16] K.P. Surendran, M.T. Sebastian, Low loss dielectrics in $Ba[(Mg_{1/3}Ta_{2/3})_{1-x}Ti_x]O_3$ and $Ba[(Mg_{1-x}Zn_x)_{1/3}Ta_{2/3}]O_3$ systems, J. Mater. Res. 20 (2005) 2919–2926.

[17] T. Shimada, Far-infrared reflection and microwave properties of $Ba([Mg_{1-x}Zn_x]_{1/3},Ta_{2/3})O_3$ ceramics, J. Eur. Ceram. Soc. 24 (2004) 1799–1803.

[18] T. Shimada, Effect of Ni substitution on the dielectric properties and lattice vibration of $Ba(Mg_{1/3}Ta_{2/3})O_3$, J. Eur. Ceram. Soc. 26 (2006) 1781–1785.

[19] M.Y. Chen, P.J. Chang, C.T. Chia, Y.C. Lee, I.N. Lin, L.J. Lin, J.F. Lee, H.Y. Lee, T. Shimada, Extended, X-ray absorption fine structure, X-ray diffraction and Raman analysis of nickel-doped $Ba(Mg_{1/3}Ta_{2/3})O_3$, J. Eur. Ceram. Soc. 27 (2007) 2995–2999.

[20] M.W. Lufaso, Crystal Structure, modelling, and dielectric property relationships of 2:1 ordered $Ba_3MM'_2O_9$ (M = Mg, Ni, Zn; M′ = Nb, Ta) perovskites, Chem. Mater. 16 (2004) 2148–2156.

[21] M. Bieringer, S.M. Moussa, L.D. Noailles, A. Burrows, C.J. Kiely, M.J. Rosseinsky, R.M. Ibberson, Cation ordering, domain growth, and zinc loss in the microwave dielectric oxide $Ba_3ZnTa_2O_{9-\delta}$, Chem. Mater. 15 (2003) 586–597.

[22] R.D. Shannon, Revised Effective ionic radii and systematic studies of interatomie distances in halides and chaleogenides, Acta Crystallogr. A 32 (1976) 751–767.

[23] A.J. Jacobson, B.M. Collins, B.E.F. Fender, A powder neutron and X-Ray diffraction determination of the structure of $Ba_3ZnTa_2O_9$: an investigation of perovskite phases in the system Ba–Ta–Zn–O and the preparation of $Ba_2TaCdO_{5.5}$ and $Ba_2CeInO_{5.5}$, Acta Crystallogr. B 32 (1976) 1083–1087.

[24] E. Kroumova, M.I. Aroyo, J.M. Perez-Mato, A. Kirov, C. Capillas, S. Ivantchev, H. Wondratschek, Bilbao crystallographic server: useful databases and tools for phase-transition studies, Phase Transitions 76 (2003) 155–170.

[25] I.N. Lin, C.T. Chia, H.L. Liu, Y.C. Chen, H.F. Cheng, C.C. Chi, High frequency dielectric properties of $Ba(Mg_{1/3}Ta_{2/3})O_3$ complex perovskite ceramics, J. Eur. Ceram. Soc. 23 (2003) 2633–2637.

[26] P.J. Chang, C.T. Chia, I.N. Lin, J.F. Lee, C.M. Lin, K.T. Wu, Characterizing $xBa(Mg_{1/3}Ta_{2/3})O_3+(1-x)Ba(Mg_{1/3}Nb_{2/3})O_3$ microwave ceramics using extended x-ray absorption fine structure method, Appl. Phys. Lett. 88 (2006) 242907.

[27] C.T. Chia, P.J. Chang, M.Y. Chen, I.N. Lin, H. Ikawa, L.J. Lin, Oxygen-octahedral phonon properties of $x BaTiO_3+(1-x)\ Ba(Mg_{1/3}Ta_{2/3})O_3$ and $xCa(Sc_{1/2}Nb_{1/2})O_3 + (1-x)Ba(Sc_{1/2}Nb_{1/2})O_3$ microwave ceramics, J. Appl. Phys. 101 (2007) 084115.

[28] S. Liu, R. Taylor, N.S. Petrovixc, L. Badd, M.V. Schilfgaarde, N. Newman, Experimental and theoretical investigation of the structural, chemical, electronic, and high frequency dielectric properties of barium cadmium tantalate-based ceramics, J. Appl. Phys. 97 (2005) 014105.